THE ASTROPHYSICAL JOURNAL, 368:570–579, 1991 February 20

IRAS LOW-RESOLUTION SPECTRAL OBSERVATIONS OF THE 10 AND 18 MICRON SILICATE EMISSION FEATURES

JANET P. SIMPSON
Astronomy Department, University of California, Berkeley, and NASA/Ames Research Center
Received 1989 January 9; accepted 1990 August 10

ABSTRACT

The *IRAS* LRS Atlas contains 8–23 μm spectra of 1816 stars with silicate emission features. In order to study the shapes of the silicate dust features, the 117 stars whose emission features appear to be optically thin and which have the best signal-to-noise ratio at the longest wavelengths were analyzed. Simple spherical dust shell models were calculated in both the optically thin and the slightly optically thick approximations. From the comparison of the predicted spectra of the dust plus stellar continuum, the emissivity function κ_λ was derived. In the different stars, the shape of the 10 μm feature is either narrow or broad and it is peaked either at $\sim$9.7 μm or at 10 μm. Either particle size effects (particles $\gtrsim$0.75 μm in radius) or optical depth effects (central optical depth $\sim$1) could broaden the 10 μm feature. Chemical composition differences no doubt are also important, particularly as regards the position of the peak of the 10 μm feature. The stars with the peak at 10 μm are more closely confined to the Galactic plane than the stars with the peak at 9.7 μm. The shape of the 18 μm feature is essentially the same in all stars, and can be used to extend the interstellar extinction curve past 13 μm to 22 μm.

Subject headings: infrared: spectra — stars: circumstellar shells

I. INTRODUCTION

Many late-type stars have large amounts of infrared emission in addition to the stellar continuum. In some cases, these infrared excesses are featureless, but in many they show strong broad emission features at 10 and 18 μm. These features have long been identified with silicate dust (see the review of Merrill 1979). The silicate dust is thought to be in a shell surrounding a cool star that is losing mass (see the reviews of Zuckerman 1980 and Jura 1985). The shape of the 10 μm feature is always smooth and broad, although there are some differences, particularly between the stellar 10 μm feature and the 10 μm feature as it appears in emission in interstellar dust such as that found in the Trapezium in the Orion Nebula (Roche and Aitken 1984). Such smooth, broad features are not characteristic of crystalline silicates, whose exact chemical compositions are well-define by the sharp substructures in their spectra. On the other hand, broad structureless 10 and 18 μm peaks are found in both magnesium and iron silicates as long as they are amorphous in structure (Day 1979, 1981; Stephens and Russell 1979) or hydrated (Zaikowski and Knacke 1975; Knacke and Krätschmer 1980). Although the 10 μm feature can be easily observed from the ground in the 8–13 μm window, the 18 μm feature can only be studied in detail from above the ground, as was done for the 10 stars (only four of which have well-defined 18 μm emission features) observed by Forrest, McCarthy, and Houck (1979) from 16 to 39 μm from the Kuiper Airborne Observatory. Like the 10 μm feature, the 18 μm feature appears to be broad, smooth, and without substructure. Terrestrial and meteoritic silicates, even amorphous ones, show more substructure than do the stellar feature, and they peak at longer wavelengths than the 18 μm feature.

The best collection of data on the 10 and 18 μm features is the spectra taken by the low-resolution spectrometer (LRS) on *IRAS*. The LRS was a prism spectrometer working from $\sim$8 μm to $\sim$22 μm, with a resolution ranging from 20 to 60 depending on wavelength. For details, see the *IRAS Explanatory Supplement 1988* (hereafter ES). Thus, this wavelength range covers both the 10 and 18 μm features at the same time and also the connecting 13–16 μm region which has hitherto been unobtainable (because of atmospheric CO_2).

In this paper, I analyze the stars with the best LRS spectra to determine the shapes of the 10 and 18 μm circumstellar silicate features. This information will be useful for future investigations of the chemistry of the dust grains, and may also help to define the interstellar absorption curve from 13 to 22 μm. There are variations in the shapes of the emission features from star to star, and these are discussed with the use of simple spherical dust shell models. Some of this variation probably does come from real variations in the chemical composition of the dust. The effects of varying the particle sizes and the optical depths will also be discussed.

II. BASIC ANALYSIS

The LRS Atlas (Atlas of Low Resolution *IRAS* Spectra 1986) contains 1816 stars in its classes 2 and 6: stars with oxygen-rich envelopes (ES). I have searched through this atlas for stars with well-defined 10 μm features and excellent signal-to-noise ratios. The definition of "well-defined" implies that the emission feature at 10 μm is optically thin or close to thin. The 117 stars so selected are listed in Tables 1–5. The identifications are from the positional associations (ES) and Gezari *et al.* (1987), and the spectral types are from the *General Catalogue of Variable Stars* (Kukarkin *et al.* 1969) and supplements, Kleinmann *et al.* (1981), Jones *et al.* (1982), and Epchtein *et al.* (1985). There are many more similar stars in the LRS Atlas, but their spectra are all noisier in the 18 μm region and so were not considered. This list of 117 stars includes the star μ Cep (IRAS 21419+5832) because it is in the LRS Atlas and because it is so well-studied in the infrared (e.g., Russell, Soifer, and Forrest 1975; Roche and Aitken 1984). In fact, its Atlas spectrum has an incorrect wavelength calibration and should not be used. The spectrum used here is an average of the correctly calibrated spectra from the LRS data base (Volk and Cohen 1989*a*

1991ApJ...368..570S

TABLE 1

Group 1—Stars with Narrow 10 μm Features

Name	LRS Char	Identification	Spectral Classification	T_0
03507+1115......	26	NML Tau =	IK Tau	500
09203−5220......	28	WY Vel	M3epIb, Irr c	600
13172+4547......	29	V CVn	M4e−M6e, SRa	750
17579+2335......	29	WY Her	M5e, Mira	600
18050−2213......	26	VX Sgr	M4e, SRa	450
20000+4954......	69	Z Cyg	M5e, Mira	487.5
21419+5832......	28	μ Cep	M2eIa, SRc	500
22345+5809......	29	W Cep	K0epIa, SRc	462.5
22480+6002......	69	AFGL 2968		337.5
23416+6130......	69	PZ Cas	M3, SRa	325

TABLE 2

Group 2—Stars with Emission Peak < 10 μm

Name	LRS Char	Identification	Spectral Classification	T_0
00042+4248......	26	KU And		400
00193−4033......	28			550
01085+3022......	29	IRC+30021		450
02351−2711......	29	IRC−30032		550
04566+5606......	27	TX Cam	Mira	462.5
05151+6312......	29	IRC+60154		512.5
05411+6957......	29	IRC+70066		525
06300+6058......	28	IRC+60169		400
07152−3444......	29	AFGL1099		600
07308+3037......	27	IRC+30187		475
07329−2352......	27	DU Pup	Mira	475
07536−2830......	28	HU Pup		375
09235−2347......	28	IRC−20188		475
09429−2148......	28	IRC−20197		375
10359−5955......	29			575
13442−6109......	27	AFGL 4178?		387.5
15226−3603......	28	AFGL 1771		437.5
15255+1944......	29	WX Ser	M8e, Mira	450
15568−4513......	29			700
16219−5048......	27			375
16222−4738......	27			325
16340−4634......	27	OH 337.9+0.3		387.5
17119+0859......	28	IRC+10322		412.5
17334+1537......	29	MW Her	Mira	525
17484−0800......	29	IRC−10381		487.5
18009−2019......	29	IRC−20424		600
18018−2802......	28	V1804 Sgr		512.5
18076−1034......	28	IRC−10401		512.5
18387−0423......	27	IRC+00363		375
18413+1354......	29	IRC+10374		450
18595−3947......	26	AFGL 5552		437.5
19042−4858......	29	U Tel	M7e, Mira	487.5
19059−2219......	28	IRC−20540		387.5
19093−3256......	28	V342 Sgr		487.5
19240+3615......	29			400
19361−1658......	29	AFGL 2425	M	412.5
19396+1637......	29	HM Sge		450
19412+0337......	29	IRC 00450		550
19422+3506......	28	AFGL 2445	M	400
19474−0744......	28	GY Aql	SR	475
19550−0201......	27	RR Aql	M6e−M7e, Mira	550
19586+3637......	29	IRC+40371		425
20042−4241......	28	V2234 Sgr		437.5
20052+0554......	29	IRC+10451		425
20135−7152......	29			450
20440−0105......	27	IRC+00490		525
20529+3013......	29	UX Cyg	M4e−M6e, Mira	600
20541−6549......	29			575
21069−3843......	29	AFGL 5592		525
22233+3013......	29	RV Peg	M6e, Mira	700

TABLE 3

Group 3—Stars with Emission Peak ≥ 10 μm

Name	LRS Char	Identification	Spectral Classification	T_0
02302+4525......	24	UX And	M6III, SRb	412.5
02469+5646......	28	W Per	M5v, Mira	375
03030+5532......	27	IO Per	M4, Irr b	425
05090−1154......	22	RX Lep	gM6, Irr b	375
06036−2411......	26	S Lep	M6, SRb	550
06278+2729......	27	DW Gem	M4, Irr b	550
08220−0821......	29	FK Hya	Mb, Irr b	625
10056−5300......	29	CM Vel	M2, SRa	550
10186−6012......	29	EV Car	M4, SRb	487.5
10226−5956......	29	CK Car	M2, SRb	550
10323−5735......	28			375
11179−6458......	29	HD 98658	M3	462.5
14003−7633......	22	θ Aps	Mbp, SRb	337.5
16418+5459......	24	S Dra	M6, SRb	425
17102−1031......	27	IRC−10359		412.5
17315−3414......	29	AFGL 5355		525
17328−3327......	29	AFGL 5357		350
17341−3453......	29	AFGL 5360		512.5
17361+5746......	28	TY Dra	M8, Irr b	512.5
17513−2313......	29	V774 Sgr	Irr b	487.5
19032−4602......	29	RX Tel	M, SRa	600
19232+5008......	26	CH Cyg	M6, SRa	1000
20194+3646......	29	BI Cyg	M4, Irr c?	437.5
21044−1637......	27	RS Cap	M4, SRb	550
21245+6221......	29	SW Cep	M6, SRb	475
22017+2806......	26	TW Peg	M7, SR	462.5
22097+5647......	29	CU Cep	M4, Mira	475
23138+6204......	27	IRC+60393		425
23504+6043......	29	TZ Cas	M2Iab, Irr c	550

TABLE 4

Group 4—Stars with Optically Thick Emission, Peak < 10 μm

Name	LRS Char	Identification	Spectral Classification	T_0
02522−5005......	24	R Hor	M7e, Mira	650
04140−8158......	24	U Men	SR	475
05052−8420......	27	V01835		550
05096−4834......	25	S Pic	M7e−M8e, Mira	650
05098−6422......	26	U Dor	M7e, Mira	487.5
05559+7430......	24	V Cam	M7e, Mira	475
06500+0829......	28	GX Mon	M9, Mira	575
07209−2540......	24	VY CMa	cM3e, Irr c	325
07304−2032......	29	Z Pup	M6e−M9e, Mira	600
16011+4722......	24	X Her	M6e, SRb	462.5
17080−3215......	28	AH Sco	M3e, SRa	450
18213+0335......	28	IRC+00349		750
18349+1023......	26	V1111 Oph		437.5
18409+1220......	28	KX Her	Mira	512.5
19244+1115......	28	IRC+10420	F8−G0 I	300
20350+3741......	29	IRC+40435		600
21270+7135......	29	IRC+70171		550
21456+6422......	28	RT Cep	M6, Mira	550
23496+6131......	27	IRC+60427		425

TABLE 5

Group 5—Stars with Optically Thick Emission, Peak ≥ 10 μm

Name	LRS Char	Spectral Identification	Classification	T_0
05367−3736......	25	RU Aur	M8e, Mira	525
06363+5954......	27	U Lyn	M8e, Mira	800
14020−3515......	29	AQ Cen	Mira	800
15576−5400......	27	HD 143183	M1−M2	487.5
17488−2800......	29	KW Sgr	Mp	487.5
20015+3019......	29	V719 Cyg	M4, Irr b	412.5
21389+5405......	24	RU Cyg	M7e, SRa	475
22142−8458......	23	SAO 258927		425
22212+5542......	26	RW Cep	M0 Ia−I, Irr c	400

and Simpson and Rubin 1990 describe the extraction procedure).

The LRS was calibrated by assuming that α Tau (spectral type K5 III) radiates as a 10,000 K blackbody (ES). Volk and Cohen (1989*b*) showed that this calibration produced stars with continua hotter than blackbodies. I have used their revised calibration to correct the shapes of the LRS spectra.

For the basic analysis, I assumed that the dust surrounds the star in an optically thin shell, a reasonable assumption considering the selection procedure. The observed flux, then, consists of the stellar continuum plus the emission from the dust grains whose temperatures depend only on their distances from the star. For the stellar continuum, I used a blackbody of 3000 K for most stars, with the exceptions IRAS 03507+1115 (NML Tau) and IRAS 19244+1115 (IRC+10420, spectral type F8–G0) which have been observed to have $T_{\rm eff}$ of 2500 and 6000 K, respectively. Even moderate errors in this temperature assumption would have little effect on the subsequent analysis since the wavelengths of the LRS are in the Rayleigh-Jeans part of the spectrum. This fitted stellar continuum should start at a wavelength short enough that there is no additional silicate dust emission (or other excess emission). From observations of μ Cep (Russell, Soifer, and Forrest 1975) over the whole range from 2 to 14 μm, it appears that the wavelength should be at least as short as 3–4 μm. On the other other hand, since most of the stars are variable, one should fit the continuum at as long a wavelength as possible in the infrared, since the flux varies less at longer wavelengths (Forrest, Gillett, and Stein 1975). Wherever possible (97 out of 117) stars, I fit the continuum to the 4 or 5 μm fluxes listed in the complication of Gezari *et al.* (1987); less than 8% gave unreasonable fits, probably because of the variability or the CO feature at 4.7 μm. Another possibility is that the overall flux calibrations of the LRS spectra are not correct (Volk and Cohen 1989*b*). I will discuss the consequences of an incorrect fitted stellar continuum later. At 7.8 μm, the stellar continuum defined by the 4 or 5 μm flux typically was found at about half the observed flux for LRS classes 27, 28, and 29, at $\frac{2}{3}$ the observed flux for classes 25 and 26, and at the observed flux level for classes 22–24. For the stars that are not in the Gezari *et al.* (1987) compilation or for the 7% where the fitted continuum was higher than the observed or practically zero at 8 μm, I fit the continuum at 7.8 μm using the above empirical result for each LRS class.

After the stellar continuum subtraction, the remaining flux is solely the emission from the dust shell. This can be written as

$$F_\lambda = \text{constant} \times \int_{R_0}^{R_{\max}} \kappa_\lambda B(T) \rho(R) 4\pi R^2 \, dR \,, \qquad (1)$$

where κ_λ is the emissivity of each dust grain, $B(T)$ is the blackbody function, T is the dust temperature at distance R from the star, and $\rho(R)$ is the dust density as a function of R. I will consider only a very simple model here, where there is no dust interior to R_0, where $R_{\max}$ is so large that there is no contribution from $B(T)$ at 24 μm, and where ρ is given by the assumption of uniform mass flow: $\rho \propto R^{-2}$. I also assume that κ_λ is not a function of the temperature of the dust, i.e., that all the dust has the same amorphous or crystalline structure, whatever the temperature. With these assumptions, one can now write

$$F_\lambda = \text{constant} \times \kappa_\lambda \int_{R_0}^{R_{\max}} B(T) \rho_0 R_0^2 4\pi \, dR = \kappa_\lambda G_\lambda \,. \qquad (2)$$

The dust temperature at any distance R from a star of temperature T_* and radius R_* is given by

$$\int_0^\infty \frac{\pi a^2 Q_{\rm abs} \pi B(T_*) 4\pi R_*^2}{4\pi R^2} \, d\lambda = \int_0^\infty 4\pi a^2 Q_{\rm abs} \pi B(T) d\lambda \,, \qquad (3)$$

where $Q_{\rm abs}$ is the efficiency for absorption or emission as a function of wavelength. The function $Q_{\rm abs}(\lambda)$ for astronomical silicate given by Draine (1985) was used and $T_* = 4000$ K. All further calculations used the normalized radius R/R_*. For example, for $T_0 = 1000$ K, $R_0 = 13R_*$. A grid of normalized model dust shells $G_\lambda = F_\lambda/\kappa_\lambda$ was produced and is given in Figure 1 for temperatures T_0 at the inner radius R_0.

The advantage of this optically thin formalization is that now I can divide each observed dust spectrum (observed flux minus stellar continuum) by the model $G_\lambda = F_\lambda/\kappa_\lambda$ and the result is the normalized dust emissivity κ_λ. The temperature T_0 was chosen for each star so that the ratio $\kappa(\lambda = 18\ \mu\text{m})/\kappa(\lambda = 10\ \mu\text{m})$ is the same for all stars. This ratio κ_{18}/κ_{10} was chosen to be 0.40, the same ratio found by Draine and Lee (1984) for astronomical silicate, although there is no *a priori* reason why it should be correct. This proceedure is significantly different from that of other researchers, who either fit a blackbody to the low points at 8 and 13 μm (e.g., Little-Marenin and Little 1988) or who assume that the temperature at the inner edge of the shell T_0 is exactly the dust condensation temperature (e.g., Skinner and Whitmore 1987). The condensation temperature for silicate dust grains is in the range 1000–1500 K (Salpeter 1977). By assuming that the inner temperature can be less than the condensation temperature, I have effectively assumed that the mass loss, and hence the dust formation, is episodic at a time scale far longer than the pulsation period, and that such a dust formation episode has not happened recently for most stars. It is also possible that the silicate dust condensation temperature is colder than 1000 K (Onaka, de Jong, and Willems 1989*a*). The reason for this different procedure is that the purpose of this study is to investigate the amount of the dust opacity, especially at wavelengths longer than 13 μm. Other authors sometimes assume the shape of the dust opacity. For example, Onaka, de Jong, and Willems

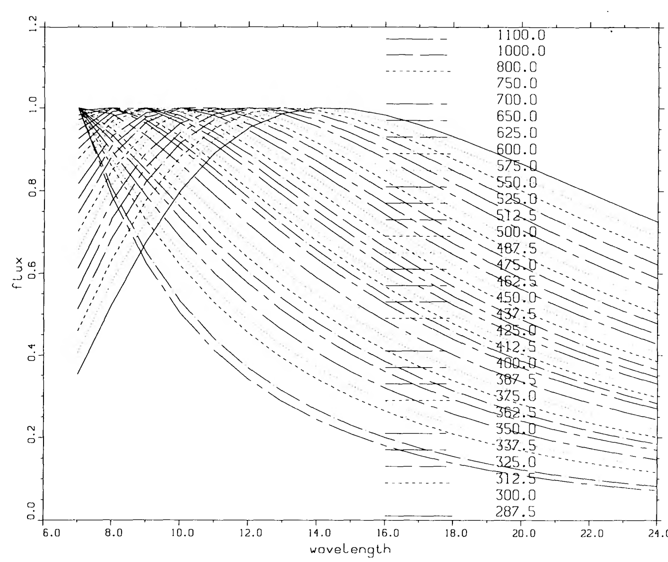

FIG. 1.—Sample dust shell models G_λ. The temperature T_0 is given for each model.

(1989*a*, 1989*b*) calculated very similar models with an assumed opacity from silicate and aluminum oxide dust in order to match the LRS spectra of Mira variables. Their fits from 9 to 13 μm are very good, but not as good from 13 to 23 μm because of their assumed opacity.

The temperatures T_0 are listed in Tables 1–5 and the resulting values of κ_λ are plotted in Figures 2–7. Changing the assumed stellar continuum can change the derived value of T_0 by $\sim$0%–10%. The effect on the derived κ_λ is shown in Figure 2, where arbitrary amounts of stellar continuum have been subtracted from the spectrum of IRAS 19232+5008. The changes are insignificant for $\lambda = 9.5$ to ~ 12 μm and $\lambda \gtrsim 16.5$ μm, and only large at ~ 8 μm, where the stellar contribution is largest.

The largest value of T_0 is 1000 K for IRAS 19232+5008 (CH Cyg) (Fig. 2). Since it is now thought that the maximum temperature to be found in a circumstellar dust shell is no more than 1000 K (Jura 1985), if the spherical dust shell model as given here is appropriate for CH Cyg, the ratio κ_{18}/κ_{10} cannot be much larger than 0.40. Of course, if the dust production is episodic instead of uniform, there might be much less dust at large distances from the star. Then dust shell models with approximately the same F_λ/κ_λ as the models in Figure 1 would have much cooler temperatures T_0 at the inner radii R_0. If the ratio κ_{18}/κ_{10} is as large as 0.45, then T_0 for CH Cyg would be 1250 K for the spherical dust shell as described above, and if the ratio is 0.50, then T_0 would be $\sim$1500 K, which is probably too high.

Comparison of the different dust emissivities, $\kappa_\lambda = F_\lambda/G_\lambda$, shows that the appearances of the dust emissivities fall into five different groups. Within each group, the dust emissivities are similar to each other with the exception of the 8–9 μm region, where κ_λ is very uncertain because of the uncertainties in the subtraction of the stellar continuum. The five groups of stars are listed in Tables 1–5 and Figures 3–7:

1. Stars with κ_{max} at $\lambda < 10$ μm and narrow 10 μm features (these include the well-studied stars μ Cep and PZ Cas (Forrest, McCarthy, and Houck 1979).

2. Stars with the 10 μm feature broader on the long wavelength side and $\lambda(\kappa_{max}) < 10$ μm.

3. Stars with the 10 μm feature broader on the long wavelength side and $\lambda(\kappa_{max}) \geq 10$ μm.

4. Stars with even broader 10 μm features than in Group 2 above, partially filling in the 14–16 μm region, and $\lambda(\kappa_{max}) < 10$ μm.

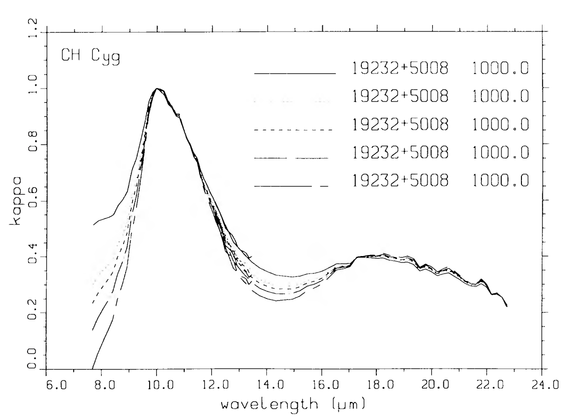

FIG. 2.—Emissivities κ_λ for CH Cyg with arbitrary amounts of stellar continuum subtracted. All the models had the same T_0.

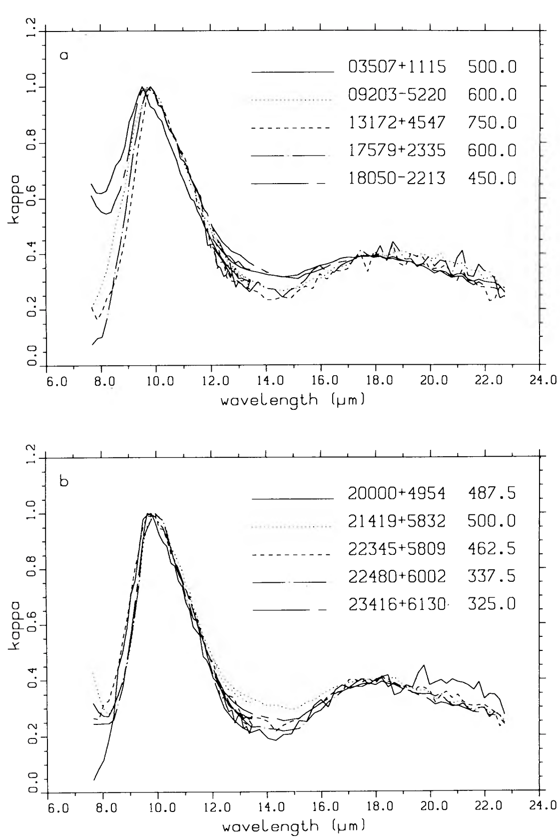

FIG. 3.—Emissivities κ_λ for Group 1. The temperature T_0 is given for each star.

5. Stars with the same broader line shape as found in Group 4, but with $\lambda(\kappa_{max}) \geq 10$ μm like Group 3.

The dust emissivities κ_λ have been averaged for each group and plotted in Figure 8. In spite of the differences in the 10 μm feature, I conclude that the 18 μm features are essentially the same. This is true for high-temperature dust shells as well as low-temperature dust shells. [The fluctuations, or wiggles in the spectra, from 19 to 22 μm are probably not real but are probably due to poor cancellation of the LRS spectral response (ES), since they appear in sources with the silicate feature in both emission and absorption and in normal A-M stars without dust shells from LRS classes 18 and 19.]

III. DISCUSSION

Simpson (1987) presented a similar analysis as in § II but using a simple λ^{-1} emissivity (or $T \propto R^{-2/5}$). If we write that the total flux from a particle is proportional to the temperature to some power α, then $\alpha = 4$ for a blackbody and $\alpha = 5$ for λ^{-1} emissivity. For Draine's (1985) Q_{abs} for a particle of radiius $a = 0.1$ μm, we find that α ranges from 4.8 at $T = 2000$ K to 3.1 at $T = 650$ K to 6.1 at $T = 50$ K. Thus it is not surprising that the values of T_0 in Tables 1–5 compared to those tabulated by Simpson (1987) differ by ≤ 50 K for $T_0 \lesssim 750$ K and are greatly different (1000 K vs. 2000 K) only for the hottest shells.

The chief reason that α falls below 4 in the temperature range 300–1300 K is that Draine's astronomical silicate is relatively transparent from ~ 1 to 8 μm compared to longer and shorter wavelengths (although not as transparent as terrestrial silicates; Draine and Lee 1984). Thus, the Wien side and the peak of the blackbody function contribute less to the total

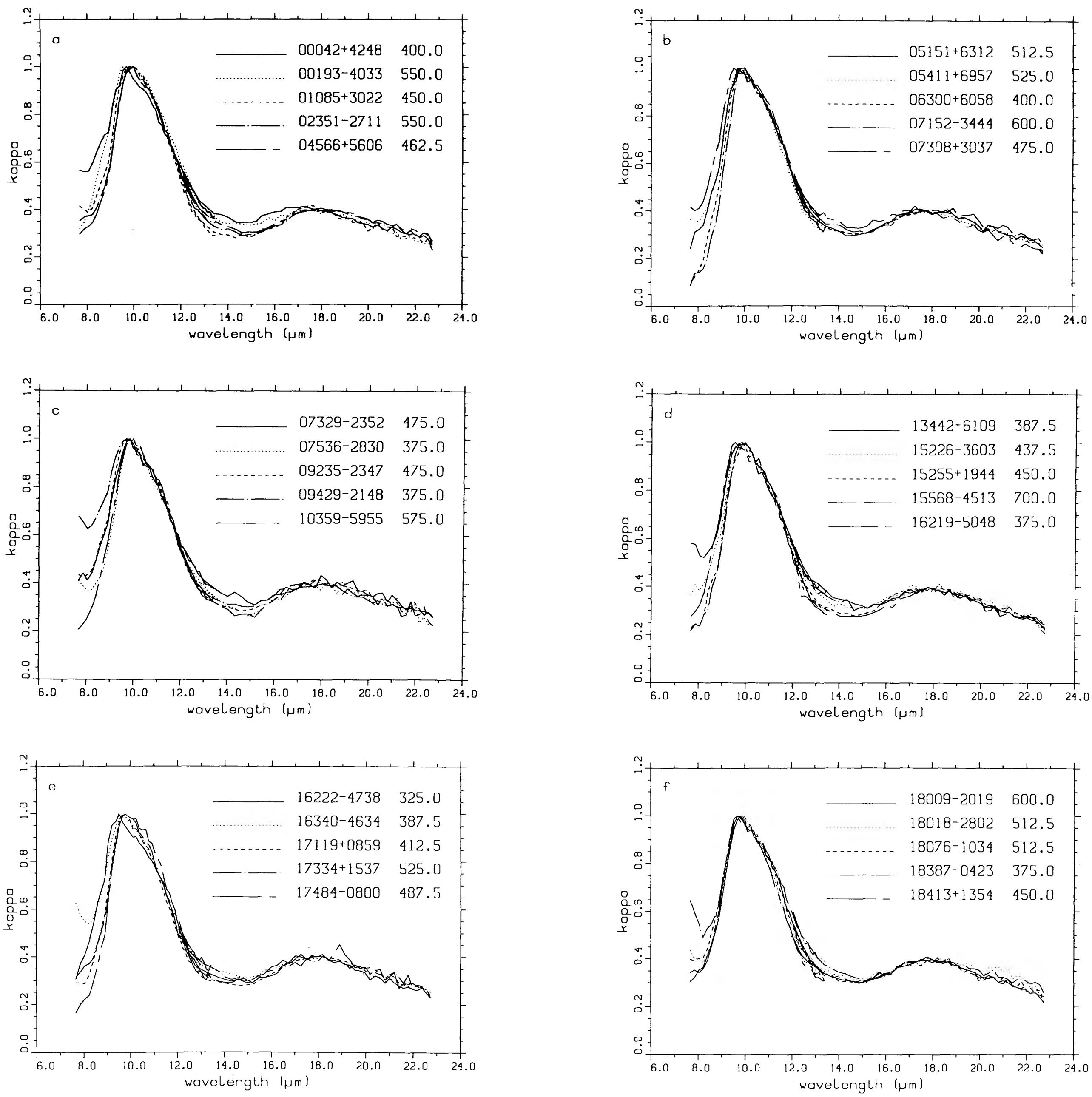

FIG. 4.—Emissivities κ_λ for Group 2

emission than they would for a gray body or a λ^{-1} emissivity. There are questions as to the relative opaqueness ("dirtyness") of astronomical silicates (including interplanetary dust—Frazier 1977; Murdock and Price 1985) compared to terrestrial silicates at visible and near-infrared wavelengths (e.g., Merrill 1979; Rogers *et al.* 1983). The problem is that if astronomical silicates are as transparent as terrestrial silicates at visible wavelengths, they will not absorb much visible light, and so will not become hot enough to radiate as much as is observed in the infrared. This problem even occurs in the 5–8 μm region, where μ Cep has excess emission (Russell, Soifer, and Forrest 1975). This excess emission cannot be due to dust if the silicates are similar to terrestrial silicates (Tsuji 1978 suggested the emission is due to H_2O in the circumstellar dust cloud), but it could be due to dust if the silicates are "dirty" enough (i.e., have a large enough imaginary part of the index of refraction k). It is certainly apparent from the figures that κ_λ is not small at 8 μm (in spite of the uncertainty) or at 14 μm, in contrast to laboratory measurements of silicates, and even Draine's (1985) astronomical silicate.

a) Position of the 10 μm *Peak*

The first question is whether the different positions of the 10 μm silicate emission peak are real. Certainly subtracting a 3000 K stellar continuum shifts the apparent peak of the silicate feature to longer wavelengths, particularly if the feature is weak and the continuum strong (LRS classes 22–25). Moreover, dividing by one of the hotter model dust shells can also

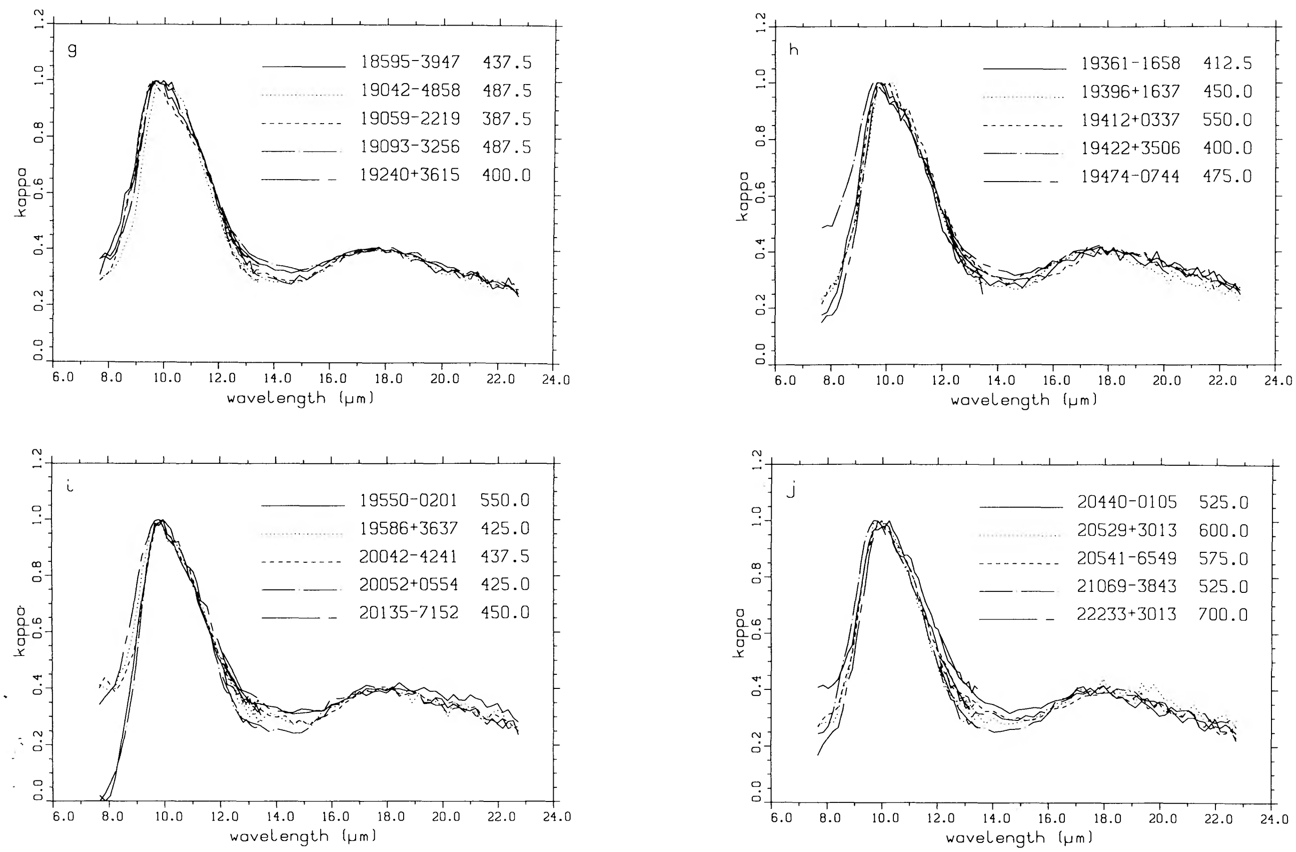

FIG. 4—*Continued*

shift the apparent peak to longer wavelengths. However, 70% of the stars in Groups 3 and 5 clearly show that the peak is at 10 μm or greater in the original LRS spectra. The wavelength calibration of each individual LRS spectra was determined from the edges of the filters (ES) rather than from the in-scan position of the source in the survey, which was less accurate. From perusal of the individual spectra in the LRS data base, I estimate that the wavelengths of point sources are good to about $\frac{1}{2}$ sample, or $\frac{1}{4}$ resolution element (one resolution element is ~ 0.3 μm at 10 μm). Moreover, each star consistently has the 10 μm feature peak at the same wavelength in all its individual spectra.

Cheeseman *et al.* (1989) have developed an artificial intelligence program for the automatic classification of LRS spectra. This program is also described by Goebel *et al.* (1989). Because they looked at all the stars in the LRS Atlas, their sample is much larger than that considered here. Their AutoClass program also finds a large class of stars with strong silicate emission features that peak at ≥ 10 μm. As a class, these stars are much more confined to the Galactic plane than are the stars whose silicate features peak at less than 10 μm. Thus, they conclude that the difference between the classes is real. Since the stars in Tables 1–5 were chosen on the basis of their good signal/noise, they are necessarily much brighter than average, and hence much closer. For this reason, many have Galactic latitudes $b \geq 10°$. However, if distances above the Galactic plane are calculated for all the stars, under the assumption that asymptotic branch giants have the same absolute magnitudes at 8 μm, the stars in Tables 2 and 4 have a significantly larger dispersion about the Galactic plane than the stars in Tables 3 and 5.

b) Width of the 10 μm *Emission Feature—Particle Size Effects*

Forrest, Gillett, and Stein (1975) were the first to suggest that the different widths of the 10 μm feature are due to different dust particle sizes. Papoular and Pégourié (1983) published detailed computations showing this effect. Figure 9 shows normalized plots of Q_{abs} (κ_λ as discussed here) calculated for spheres of radius a using a Mie scattering program. Draine's (1985) values of the complex index of refraction for astronomical silicate were used. Because of the very sharp increase of the imaginary part of the index of refraction as λ increases from 7.5 to 9 μm, there is no broadening at the short wavelength side of the 10 μm feature for particles with a up to ~ 1 μm. However, the 10 μm feature is substantially broadened on the long wavelength side as the individual particle becomes optically thick with increasing radius. Thus the idea that some dust shells contain particles larger than the canonical 0.1 μm is consistant with the LRS data.

c) Width of the 10 μm *Emission Feature—Optical Depth Effects*

A finite optical depth can also cause the 10 μm feature to appear broader than an optically thin feature. I will discuss this in terms of IRC + 10420 (IRAS 19244 + 1115), a star in Group 4. Dyck *et al.* (1984), Ridgway *et al.* (1986), Cobb and Fix (1987), and Fix and Cobb (1988) present speckle interferometer measurements of the diameter of IRC + 10420 from 2 to 10 μm. The short-wavelength measurements mainly see the star and

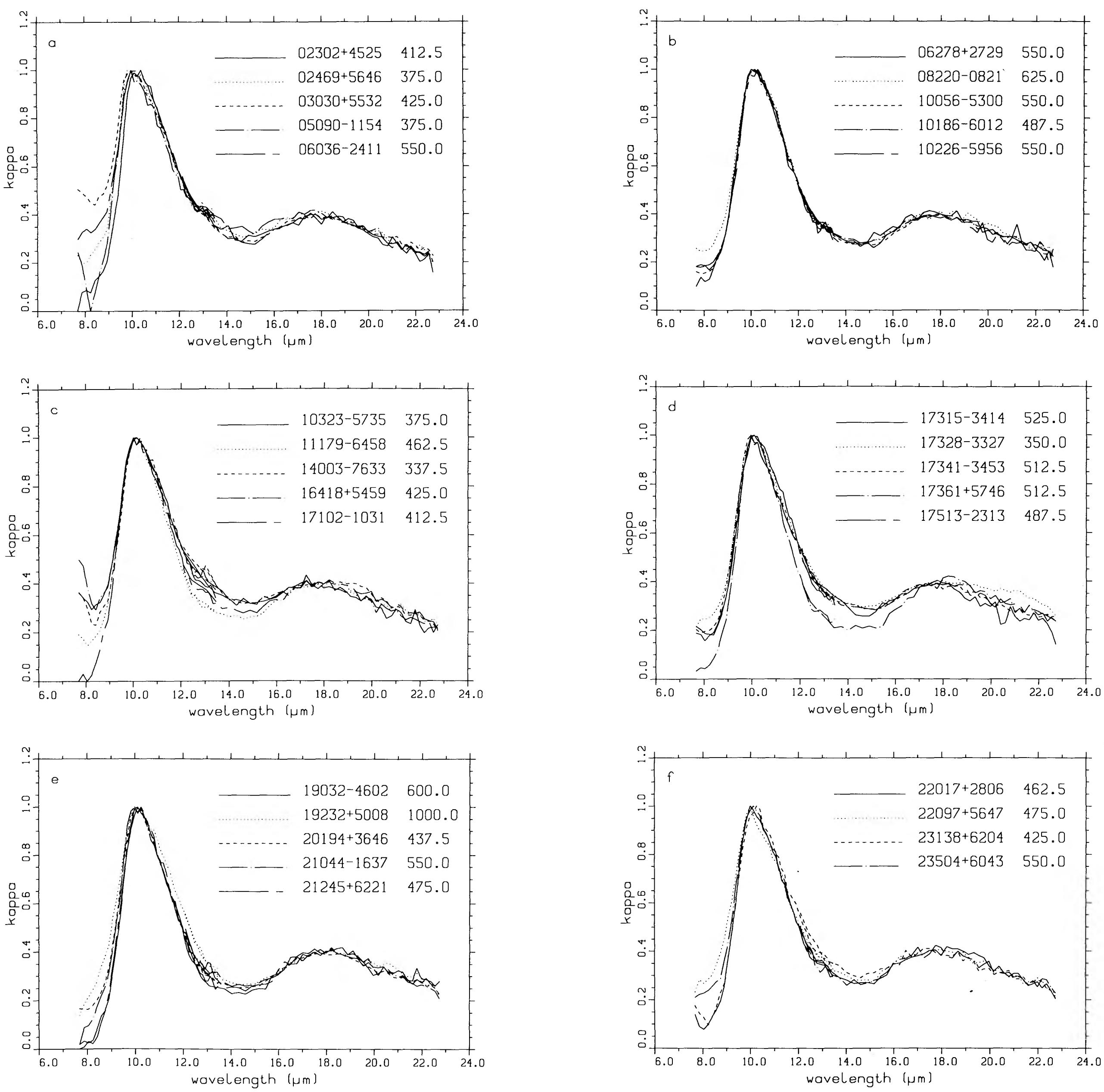

FIG. 5.—Emissivities κ_λ for Group 3

hot dust, but the 10 μm measurements are mainly of the dust shell. A good fit must include both the absolute flux at all wavelengths and the angular diameter. The simple spherical dust shell models cannot, in fact, fit all the interferometry data at all wavelengths, but consideration of them is very instructive.

The dust shell models were calculated for the slightly optically thick case with no interstellar absorption. In the slightly optically thick approximation, the dust in the shell absorbs the infrared radiation on its way to the telescope, but the temperature structure of the dust shell is the same as the temperatures in the optically thin case. (Under a detailed radiative transfer calculation, the dust temperatures at large radii from the star would be cooler than under the slightly optically thick approximation, but about the same at R_0.) The largest optical depth considered here was ~ 1.2 between the star and the outside of the shell at the 10 μm peak. Figure 3 of Jones and Merrill (1976) plots dust temperatures for models with $\tau_{10\,\mu\mathrm{m}} = 6.0$, a more extreme case than considered here. For these models, κ_λ was the value derived for the Group 1 emission stars (Fig. 8).

For each model, I calculated the visibility amplitude at 8.7 and 9.8 μm, the wavelengths of the best data of Fix and Cobb (1988). The appropriate visibility function is given by a one-dimensional Fourier transform of the strip intensity distribution, since the observations were made by scanning a slit (Ridgway *et al.* 1986); it is necessary to include the point source contribution of the star itself in the strip intensity. The dust shell models do not have the appearance of a Gaussian (the visibility function of a Gaussian is also a Gaussian and is

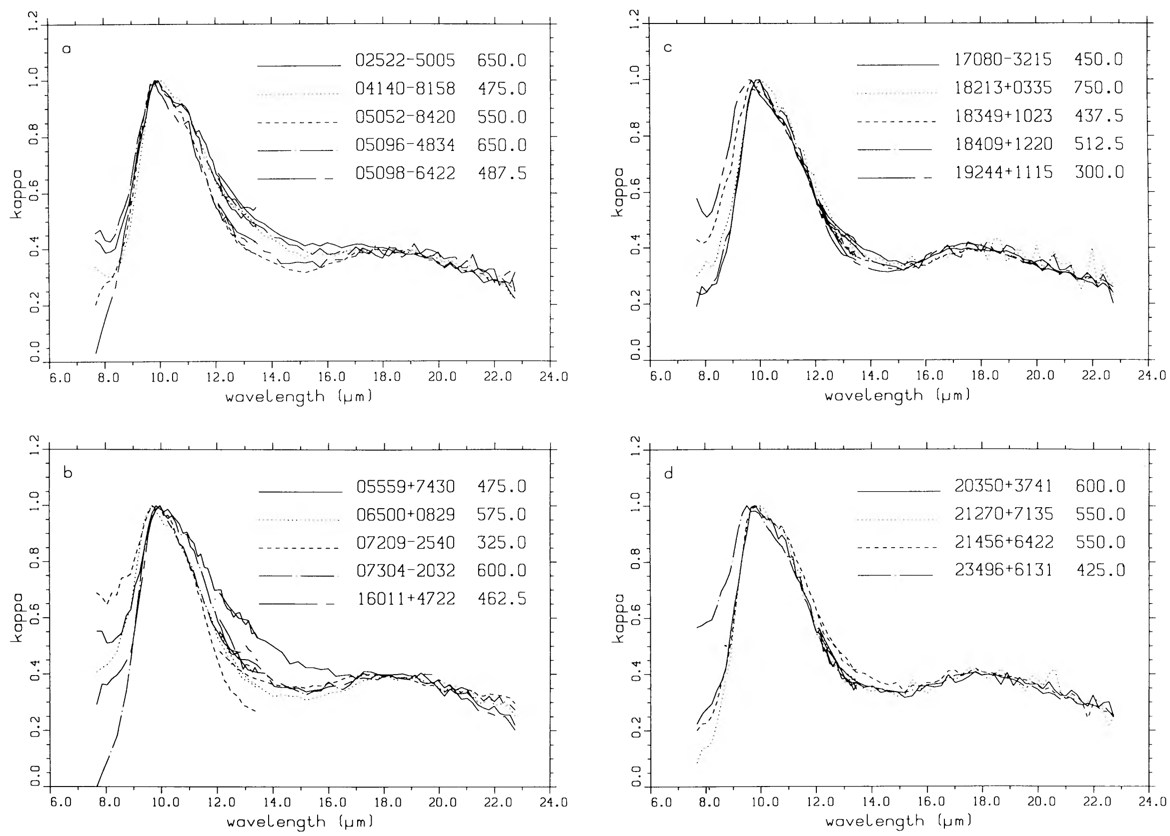

FIG. 6.—Emissivities κ_λ for Group 4

commonly fit to observed data for the estimation of a source size), but it is better described by a narrow core with a halo. The corresponding visibility function is much broader than that of the Gaussian with the same full width at half-maximum (FWHM) and it is relatively flatter, especially when an additional point source is included. Good fits to the visibility functions at all wavelengths could not be obtained unless a fairly substantial point source was added to the source profile. This point source could include emission from very hot dust in the immediate vicinity of the star, as well as the star itself. Also, the FWHM of the model had to be larger than the FWHM of the Gaussian that best fit the visibility data in order to produce enough total flux. A reasonable (but not unique) fit could be found to both the visibility data of Fix and Cobb (1988) at 8.7 μm (except for the two highest frequency points) and the *IRAS* data for the model with $T_0 = 350$ K and FWHM = 0″45. However, the visibility data at 9.8 μm have the same width as at 8.7 μm, and thus the larger contribution from the cool dust at large distances from the star requires a point source contribution of $\sim$33% for a good fit. The 10 μm N filter visibility amplitude measurement of Cobb and Fix (1987) is somewhat narrower, but still wider than the calculated amplitude, and thus point source contributions must be included. The star does not contribute more than 5%–12% of the total flux at these wavelengths if the continuum at 4.8 μm (Thomas, Robinson, and Hyland 1976) is entirely due to the star, and less if the 4.8 μm continuum includes contributions from the dust shell (Forrest, McCarthy, and Houck 1979; Ridgway *et al.* 1986). Ridgway *et al.* (1986) also had to add a 40% point source contribution to match the visibility data at 5 μm. The flux scale for IRC+10420 in the LRS Atlas is about 25% lower than the *IRAS* 12 μm point source flux (*IRAS Point Source Catalog, Version 2 1988*). If the model used the 12 μm point source catalog flux, as suggested by Volk and Cohen (1989*b*), instead of the lower LRS flux, an additional point source contribution of 30% would be necessary to match the 8.7 μm visibility and 50% for the 9.7 μm visibility. We note that at 20 μm, the LRS flux is much smaller than the flux observed by Forrest, McCarthy, and Houck (1979).

A possible reason for the discrepancy between the observations and the model predictions is that the smooth, spherically symmetric dust shell model is too simple. Other models are discussed by Cobb and Fix (1987). For example, some dust much hotter than 350 K must be present to account for the visibility measurements at 5 μm of Ridgway *et al.* (1986). Also, Bowers (1984) prefers a clumpy distribution from VLA observations of OH masers.

The dust shell spectrum of IRC+10420 produced by this model is plotted in Figure 10, along with the observed LRS data. It is seen that with the addition of some optical depth, the narrow Group 1 opacity produces a 10 μm feature that is as wide as the observed Group 4 feature. I conclude that, at least in some cases, a broad 10 μm feature can be caused by optical depth effects. In other cases, where the star can be clearly seen at visible wavelengths, either the dust is not optically thick or the geometry is not represented by a uniform spherical shell.

d) *Other Variations*

It is clear that there must be some variation in the chemical composition of the dust shells in order to explain the variations

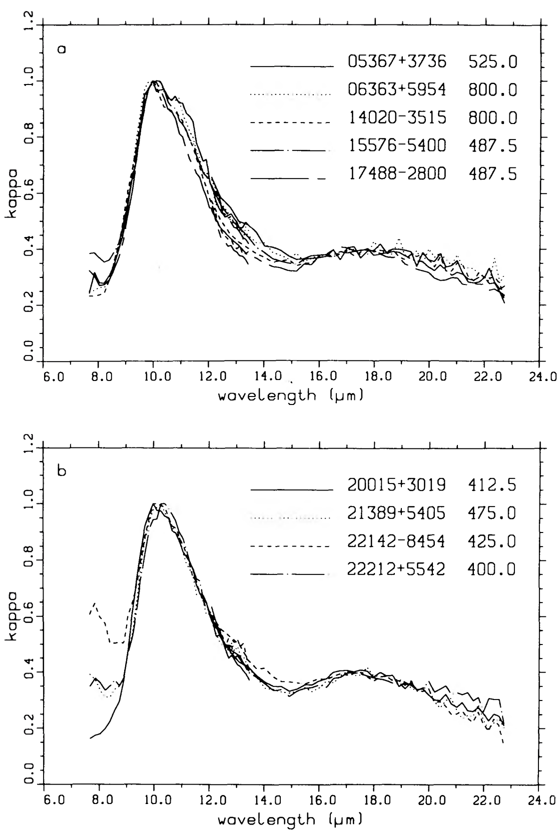

FIG. 7.—Emissivities κ_λ for Group 5

in the wavelength and width of the peak of the 10 μm feature. For example, the dust emission feature in the Trapezium of the Orion Nebula (Forrest, Gillett, and Stein 1975) has the same peak as the Group 1 feature as seen in μ Cep with no broadening on the long-wavelength side (as might be explained by particle size effects or optical depth effects), but it is broader on the short-wavelength side. (We note that, compared to the 10 μm peak, the LRS spectrum of μ Cep has more emission at 13 μm than the spectrum of Russell *et al.* 1975; the short wavelength continuum is also higher.) (The 10 μm feature would be narrower on the long wavelength side if a colder dust model were used, and the κ_{18}/κ_{10} ratio were less than 0.35.) Two stars in Group 1 with this short a wavelength cut-on are NML Tau and WY Vel. A star with a much *narrower* feature at 10 μm is α

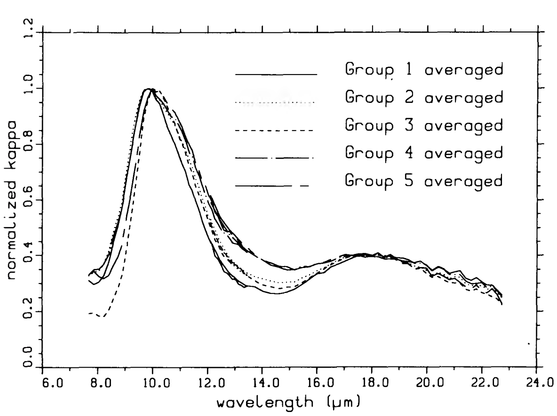

FIG. 8.—The emissivities averaged for each group

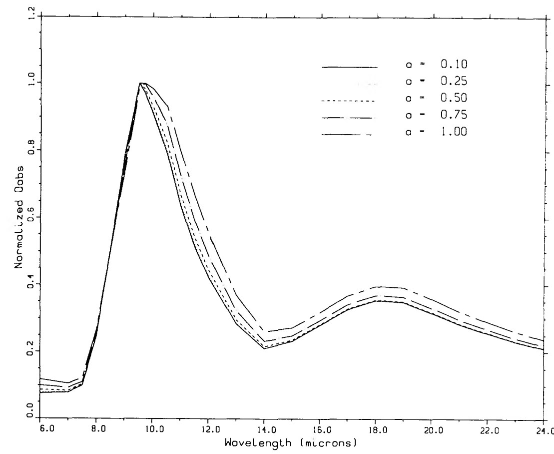

FIG. 9.—Mie calculations of $Q_{\rm abs}$ for silicate particles of radius a in μm. Note that the 10 μm feature is broadened at longer wavelengths as the particle size increases.

Ori (IRAS 05524+0723); since there is only one member in this "group," it was not included in this study. However, the 18 μm feature does look like that of the other stars if a model with $T_0 = 450$ K is used. With such a low temperature, it is not necessary to require a chromosphere (Skinner and Whitmore 1987) to get a reasonable flux at 20 μm.

The silicate dust emission feature in the Trapezium (Forrest, Gillett, and Stein 1975) is very similar to the feature in Group 1 (the narrowest) from 9.7 to 13 μm but is broader from 8 to 9.7 μm. The absorption coefficient derived from the Trapezium emission feature gives good agreement with the 10 μm absorption in protostars, molecular clouds, and H II regions (Gillett *et al.* 1975; Willner 1977). However, Roche and Aitken find that the interstellar absorption toward the Galactic center (1985) and toward Wolf-Rayet stars (1984) is better given by the shape of the μ Cep feature. Although there is a lot of variation among the groups from 8 to 15 μm, the 18 μm feature is very similar in all the groups. It is possible, then, that the interstellar absorption coefficient from 12–23 μm could be described by the shape of the κ_λ derived for Group 1.

The exact chemical composition of the dust is not known. Laboratory measurements of amorphous silicates (Day 1979,

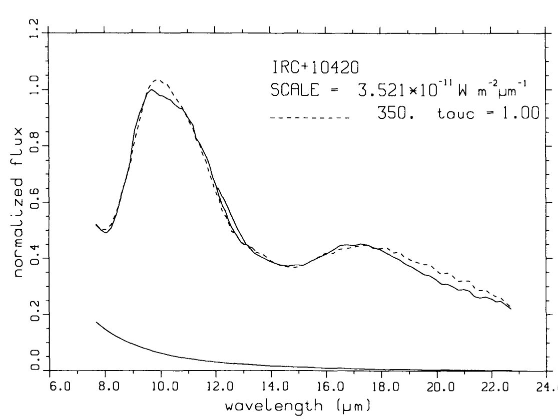

FIG. 10.—LRS spectrum of IRC+10420. The upper solid curve is the total observed flux (scaled by 3.521×10^{11} W m^{-2} μm^{-1}) and the lower solid curve is the flux of a 6000 K blackbody, fit to the measured flux of Thomas, Robinson, and Hyland (1976) at 4.8 μm. The dashed line is the slightly optically thick dust shell model described in the text plus the 6000 K blackbody (the stellar contribution).

1981) show broad, smooth features that peak at 9.5–10 μm and 19–20 μm. Likewise, carbonaceous chondrite meteorites and hydrated silicates (Knacke and Krätschmer 1980) have 10 μm features that look similar to the features described here, but the 18 μm feature peaks at a much longer wavelength than is observed in the circumstellar dust shells and shows considerable structure as well. Pégourié and Popular (1985) and Papoular and Pégourié (1986) discuss the formation of dust grains of these materials. Onaka, de Jong, and Willems (1989*a*, *b*) and Stencel *et al.* (1990) suggest that young dust shells contain aluminum oxide, which has a smooth feature at 12 μm. This feature could be the cause of the apparent "broadening" of the 10 μm feature, instead of particle size or optical depth.

IV. SUMMARY

The *IRAS* LRS Atlas was searched for stars with strong well-defined silicate emission features at 10 and 18 μm. These spectra were divided by synthetic spectra from simple models of optically thin spherical dust shells with the emissivity function κ_λ removed from under the integral sign. The result was the normalized emissivities κ_λ, which were plotted and compared. The 18 μm features appear basically the same in all the stars, but there are differences in the 10 μm features. The 10 μm features vary in width and the position of the peak varies from <9.7 to ~ 10 μm. The stars with the 10 μm peak at longer wavelength seem to be more closely confined to the Galactic plane. At the resolution of the LRS, there is never any substructure visible in either the 10 or 18 μm features that would indicate crystalline structure for the dust, regardless of the temperature of the dust in the shell.

Simple models were calculated for slightly optically thick dust shells. These models have broader 10 μm features than the optically thin models; such models can be fit to at least some of the stars whose dust shells have broad 10 μm features, although the broadening caused by a finite optical depth occurs on both the short and the long wavelength side of the feature. On the other hand, Mie calculations of the absorptivity (emissivity) $Q_{\rm abs}$ for Draine's (1985) astronomical silicate shown broadening only on the long wavelength side of the 10 μm peak as the particle radius increases from ~ 0.25 μm to >1.0 μm. Thus the different shapes could be explained if the different stars have a variety of particle sizes or optical depths. There must also be a variation in chemical composition as well.

The observed interstellar extinction in diffuse regions (such as is found between the Sun and the Galactic center) is well-described by the shape of the 10 μm feature as found in the group with the narrowest feature (Group 1). The peak is at ~ 9.7 μm. Thus, the κ_λ for 12–23 μm for the Group 1 stars may also be a good representation for the interstellar extinction for those wavelengths, especially since the 18 μm feature does not vary even when the 10 μm feature varies.

This work was supported (in part) by the *IRAS* General Investigator Program and by NASA Ames Research Center Interchange Grant NCC2-548. I thank P. Swann and G. Villere for their help in accessing the LRS data before publication of the Atlas, and G. Augason, M. Cohen, J. Goebel, R. Rubin, and H. Walker for helpful discussions, and P. Wesselius for providing the Gronigen LRS data base. Finally, I thank the anonymous referee for his thoughtful comments.

REFERENCES

Atlas of Low Resolution *IRAS* Spectra 1986, *IRAS* Science Team, prepared by F. M. Olnon and E. Raimond, *Astr. Ap. Suppl.*, **65**, 607.
Bowers, P. F. 1984, *Ap. J.*, **279**, 350.
Cheeseman, P., Stutz, J., Self, M., Taylor, W., Goebel, J., Volk, K., and Walker, H. 1989, *Automatic Classification of Spectra From the Infrared Astronomical Satellite* (*IRAS*), NASA Reference Publication 1217.
Cobb, M. L., and Fix, J. D. 1987, *Ap. J.*, **315**, 325.
Day, K. L. 1979, *Ap. J.*, **234**, 158.
———. 1981, *Ap. J.*, **246**, 110.
Draine, B. T. 1985, *Ap. J. Suppl.*, **57**, 587.
Draine, B. T., and Lee, H. M. 1984, *Ap. J.*, **283**, 89.
Dyck, H. M., Zuckerman, B., Leinert, C., and Beckwith, S. 1984, *Ap. J.*, **287**, 801.
Epchtein, N., *et al.* 1985, *Astr. Ap. Suppl.*, **61**, 203.
Fix, J. D., and Cobb, M. L. 1988, *Ap. J.*, **329**, 290.
Forrest, W. J., Gillett, F. C., and Stein, W. A. 1975, *Ap. J.*, **195**, 423.
Forrest, W. J., McCarthy, J. F., and Houck, J. R. 1979, *Ap. J.*, **233**, 611.
Frazier, E. N. 1977, *Infrared Radiation of the Zodiocal Light* (SPIE Proc., vol. **124**), p. 139.
Gezari, D. Y., Schmitz, M., and Mead, J. L. 1987, *Catalog of Infrared Observations*, NASA Reference Publication 1196.
Gillett, F. C., Forrest, W. J., Merrill, K. M., Capps, R. W., and Soifer, B. T. 1975, *Ap. J.*, **200**, 609.
Goebel, J. H., Volk, K., Walker, H., Gerbault, F., Cheeseman, P., Self, M., Stutz, J., and Taylor, W. 1989, *Astr. Ap.*, **222**, L5.
IRAS Catalogs and Atlases: Explanatory Supplement 1988, ed. C. A. Beichman, G. Neugebauer, H. J. Habing, P. E. Clegg, and T. J. Chester (Washington, DC: GPO) (ES).
IRAS Point Source Catalog, Version 2 1988, Joint *IRAS* Science Working Group (Washington, DC: GPO).
Jones, T. W., Hyland, A. R., Caswell, J. L., and Gatley, I. 1982, *Ap. J.*, **253**, 208.
Jones, T. W., and Merrill, K. M. 1976, *Ap. J.*, **209**, 509.
Jura, M. 1985, *Interrelationships Among Circumstellar, Interstellar, and Interplanetary Dust*, ed. J. A. Nuth III and R. E. Stencel, NASA CR 2403, p. 3.
Kleinmann, S. G., Gillett, F. C., and Joyce, R. R. 1981, *Ann. Rev. Astr. Ap.*, **19**, 411.
Knacke, R. F., and Krätschmer, W. 1980, *Astr. Ap.*, **92**, 281.
Kukarkin, B. V., *et al.* 1969, *General Catalogue of Variable Stars* (3d ed. and later supplements; Moscow: Astr. Council Acad. Sci. USSR).
Little-Marenin, I. R., and Little, S. J. 1988, *Ap. J.*, **333**, 305.
Merrill, K. M. 1979, *Ap. Space Sci.*, **65**, 199.
Murdock, T. L., and Price, S. D. 1985, *A.J.*, **90**, 375.
Onaka, T., de Jong, T., and Willems, F. J. 1989*a*, *Astr. Ap.*, **218**, 169.
———. 1989*b*, *Astr. Ap. Suppl.*, **81**, 261.
Popoular, R., and Pégourié, B. 1983, *Astr. Ap.*, **128**, 335.
———. 1986, *Astr. Ap.*, **156**, 199.
Pégourié, B., and Papoular, R. 1985, *Astr. Ap.*, **142**, 451.
Ridgway, S. T., Joyce, R. R., Conners, D., Pipher, J. L., and Dainty, C. 1986, *Ap. J.*, **302**, 662.
Roche, P. F., and Aitken, D. K. 1984, *M.N.R.A.S.*, **208**, 481.
———. 1985, *M.N.R.A.S.*, **215**, 425.
Rogers, C., Martin, P. G., and Crabtree, D. R. 1983, *Ap. J.*, **272**, 175.
Russell, R. W., Soifer, B. T., and Forrest, W. J. 1975, *Ap. J. (Letters)*, **198**, L41.
Salpeter, E. E. 1977, *Ann. Rev. Astr. Ap.*, **15**, 267.
Simpson, J. P. 1987, poster paper presented at From Comets to Cosmology, Third Int. *IRAS* Conference, July 6-10, 1987, Queen Mary College, London.
Simpson, J. P., and Rubin, R. H. 1990, *Ap. J.*, **354**, 165.
Skinner, C. J., and Whitmore, B. 1987, *M.N.R.A.S.*, **224**, 335.
Stencel, R. E., Nuth, J. A. III, Little-Marenin, I. R., and Little, S. J. 1990, *Ap. J. (Letters)*, **350**, L45.
Stephens, J. R., and Russell, R. W. 1979, *Ap. J.*, **228**, 780.
Thomas, J. A., Robinson, G., and Hyland, A. R. 1976, *M.N.R.A.S.*, **174**, 711.
Tsuji, T. 1978, *Astr. Ap.*, **68**, L23.
Willner, S. P. 1977, *Ap. J.*, **214**, 706.
Volk, K., and Cohen, M. 1989*a*, *A.J.*, **98**, 931.
———. 1989*b*, *A.J.*, **98**, 1918.
Zaikowski, A., and Knacke, R. F. 1975, *Ap. Space Sci.*, **37**, 3.
Zuckerman, B. 1980, *Ann. Rev. Astr. Ap.*, **18**, 263.

JANET P. SIMPSON: Astrophysical Experiments Branch, MS 245-6, NASA/Ames Research Center, Moffett Field, CA 94035